ADVANCED MATERIALS

Intrinsically stretchable light-emitting diodes (ISOLEDs) are becoming increasingly important for wearable electronics. In article number 2203040, Han-Young Woo, Tae-Woo Lee, and co-workers report the design of highly efficient ISOLEDs that use a graphene-based 2D-contact stretchable electrode. As a benefit of a newly designed conjugated polyelectrolyte with efficient electron injection capability, the ISOLED yields an unprecedently high current efficiency of 20.3 cd A^{-1}.

ORGANIC LIGHT-EMITTING DIODES

Graphene-Based Intrinsically Stretchable 2D-Contact Electrodes for Highly Efficient Organic Light-Emitting Diodes

Huanyu Zhou, Shin Jung Han, Amit Kumar Harit, Dong Hyun Kim, Dae Yoon Kim, Yong Seok Choi, Hyeokjun Kwon, Kwan-Nyeong Kim, Gyeong-Tak Go, Hyung Joong Yun, Byung Hee Hong, Min Chul Suh, Seung Yoon Ryu, Han Young Woo,* and Tae-Woo Lee*

Intrinsically stretchable organic light-emitting diodes (ISOLEDs) are becoming essential components of wearable electronics. However, the efficiencies of ISOLEDs have been highly inferior compared with their rigid counterparts, which is due to the lack of ideal stretchable electrode materials that can overcome the poor charge injection at 1D metallic nanowire/organic interfaces. Herein, highly efficient ISOLEDs that use graphene-based 2D-contact stretchable electrodes (TCSEs) that incorporate a graphene layer on top of embedded metallic nanowires are demonstrated. The graphene layer modifies the work function, promotes charge spreading, and impedes inward diffusion of oxygen and moisture. The work function (WF) of 3.57 eV is achieved by forming a strong interfacial dipole after deposition of a newly designed conjugated polyelectrolyte with crown ether and anionic sulfonate groups on TCSE; this is the lowest value ever reported among ISOLEDs, which overcomes the existing problem of very poor electron injection in ISOLEDs. Subsequent pressure-controlled lamination yields a highly efficient fluorescent ISOLED with an unprecedentedly high current efficiency of 20.3 cd A^{-1}, which even exceeds that of an otherwise-identical rigid counterpart. Lastly, a 3 inch five-by-five passive matrix ISOLED is demonstrated using convex stretching. This work can provide a rational protocol for designing intrinsically stretchable high-efficiency optoelectronic devices with favorable interfacial electronic structures.

1. Introduction

Wearable electronics require integrated devices that can stretch to form intimate contact with human skin.[1–9] DC-driven intrinsically stretchable organic light-emitting diodes (ISOLEDs) that have high efficiency are particularly promising for wearable applications.[10–16] However, since 2011 only a few papers have reported ISOLEDs, and they have not achieved high current efficiency (CE) >12 cd A^{-1}, whereas rigid counterparts that use an indium tin oxide (ITO) anode and a metal cathode even have CE ≈20 cd A^{-1}.[17,18] The low CE of ISOLEDs can be ascribed to the lack of stretchable electrode materials that can solve the poor charge injection at the widely used 1D metallic nanowire/organic layer interface. Furthermore, protocols related to ISOLEDs fabrication and optimization process have not been established, so the task of boosting ISOLED efficiency is extremely challenging.

H. Zhou, S. J. Han, H. Kwon, K.-N. Kim, G.-T. Go, T.-W. Lee
Department of Materials Science and Engineering
Seoul National University
Seoul 08826, Republic of Korea
E-mail: twlees@snu.ac.kr

A. K. Harit, H. Y. Woo
Department of Chemistry
KU-KIST Graduate School of Converging Science and Technology
Korea University
Seoul 02841, Republic of Korea
E-mail: hywoo@korea.ac.kr

D. H. Kim, S. Y. Ryu
Division of Display and Semiconductor Physics
Display Convergence
College of Science and Technology
E-ICT–Culture-Sports Convergence Track
Korea University
Sejong Campus, Sejong City 30019, Republic of Korea

D. Y. Kim, Y. S. Choi, B. H. Hong
Graphene Square Inc.
Suwon 16229, Republic of Korea

H. J. Yun
Advanced Nano Research Group
Korea Basic Science Institute (KBSI)
Daejeon 34126, Republic of Korea

B. H. Hong
Department of Chemistry
Seoul National University
Seoul 08826, Republic of Korea

M. C. Suh
Department of Information Display
Kyung Hee University
Seoul 02447, Republic of Korea

T.-W. Lee
School of Chemical and Biological Engineering
Institute of Engineering Research
Research Institute of Advanced Materials
Soft Foundry
Seoul National University
Seoul 08826, Republic of Korea

Embedded silver nanowires (AgNWs) have been widely used as stretchable electrodes.[19,20] However, the contact area is limited at the 1D AgNW/organic layer interface, so the embedded AgNWs have poor charge-injection properties. Energy-level misalignment at stretchable electrode/organic interfaces of ISOLEDs is another problem that must be solved. Especially, efficient electron injection is difficult to attain in solution-processed ISOLEDs without using reactive alkali fluorides or metals (e.g., Ca, Ba, Cs, LiF, BaF$_2$, or CsF) as the interlayer.[21] A recent stretchable electrode that has low work function (WF) showed only WF $\approx$4.7 eV which is not suitable for efficient electron or hole injection at the cathode or the anode, respectively.[4] Hence, to boost the efficiency of ISOLED, energy levels must be aligned at both the stretchable electrode interfaces.

This paper reports a highly efficient ISOLED that uses 2D-contact stretchable electrodes (TCSEs) as the anode and cathode (**Figure 1**A). The TCSE includes a layer of graphene and graphene scrolls on top of embedded AgNW networks in the styrene–ethylene–butadiene–styrene (SEBS) elastomer matrix. The graphene layer modifies the WF, promotes charge spreading, and impedes inward diffusion of oxygen and moisture, and thereby achieving significant improvement in charge injection and environmental stability. The electron injection property of the cathode TCSE can be substantially increased by introducing an anionic crown conjugated polyelectrolyte (CPE) interlayer that induces a strong interfacial dipole to yield

a low WF = 3.57 eV which is the lowest value ever reported among ISOLEDs. Subsequent p-type molecular doping of the anode TCSE establishes efficient hole injection with a high WF = 5.69 eV. The mechanical stability of the TCSEs is improved due to the graphene scrolls that bridge the cracks and graphene oxide (GO) that bind the NW–NW junctions. With all these benefits, the pressure-controlled lamination process yielded efficient charge injection, and a highly efficient ISOLED with CE = 20.3 cd A^{-1}. Furthermore, a three-inch five-by-five passive matrix ISOLED successfully withstood convex deformation.

2. Results and Discussion

SEBS was chosen as the elastomer matrix for the TCSE other than the widely used poly(dimethylsiloxane) (PDMS) due to its high miscibility with the poly(vinylpyrrolidone) (PVP), the polymer ligand that wraps the AgNW during the synthesis; this can be confirmed with the estimation of Hansen solubility parameter (Table S1, Supporting Information, calculated as reported previously[22]). However, lateral charge transport in pristine AgNW percolated networks is confined within the NWs, and charge transport between wires is only allowed at NW–NW junctions; the severity of this limitation increases after AgNWs are embedded with a limited electrical contact area within the
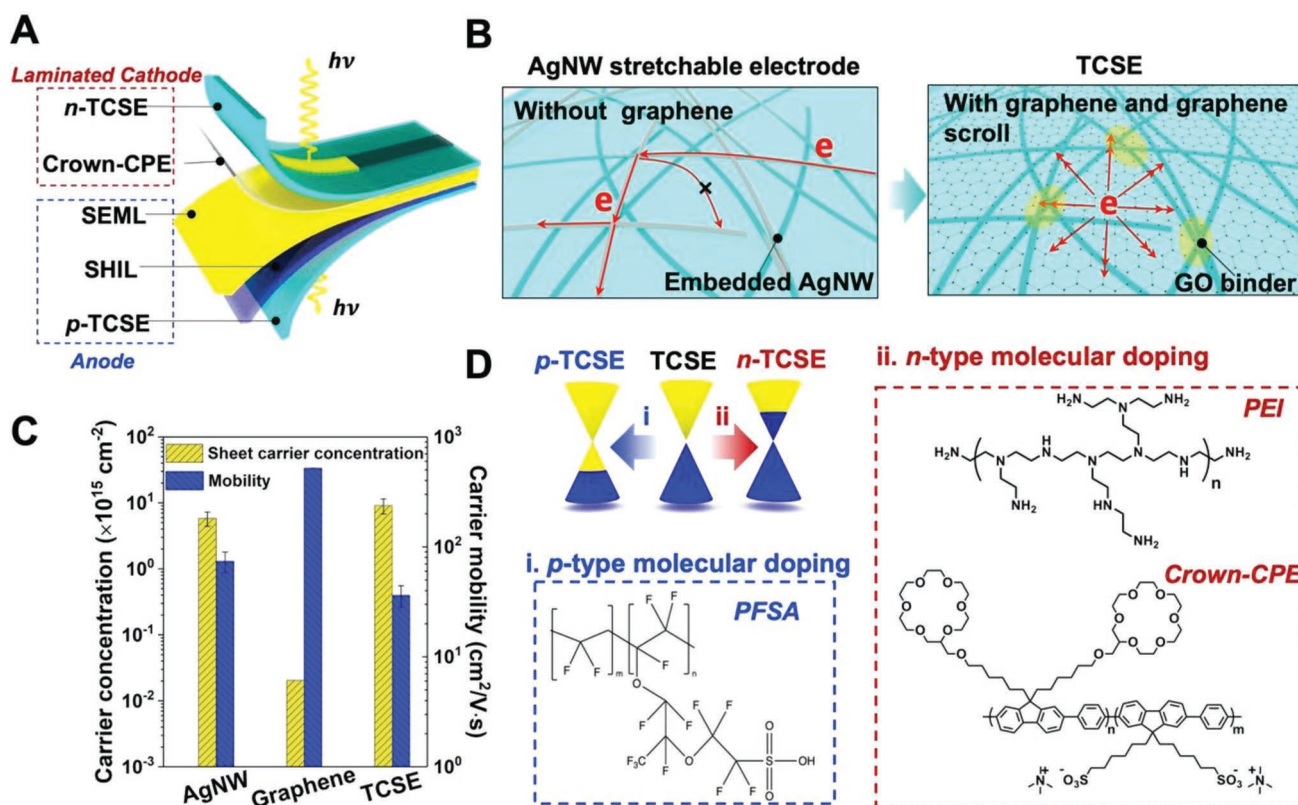

Figure 1. A) Conceptual illustration of the ISOLED based on p- and n-doped 2D-contact stretchable electrodes (TCSEs). B) Schematic of the pristine silver nanowire (AgNW) and TCSE. C) Sheet carrier concentration and carrier mobility of AgNW, graphene, and TCSE evaluated using Hall effect measurement. D) Materials used for p-type or n-type molecular doping of TCSEs. Perfluorosulfonic acid (PFSA) in a blue dashed rectangle for p-type molecular doping; PEI, and Crown-CPE in red for n-type TCSEs. SHIL: stretchable hole-injection layer; SEML: stretchable light-emitting layer.

**ADVANCED
SCIENCE NEWS**

www.advancedsciencenews.com

**ADVANCED
MATERIALS**

www.advmat.de

elastomer matrix (Figure 1B). To solve this problem, the surface of the TCSE was covered with a graphene layer, which formed a complete 2D contact at the interface between the TCSE and the adjacent organic layer. Hence, a reliable 2D-electrical contact for ISOLED can be achieved.

The charge-carrier properties of graphene as a charge-spreading promoter were confirmed by measuring the Hall effect. Carrier mobility was higher $\mu = 519.27$ cm^2 V^{-1} s^{-1} in graphene layer than in pristine AgNW networks ($\mu = 73.39$ cm^2 V^{-1} s^{-1}) (Figure 1C). Furthermore, the surface carrier density $n = 9.10 \times 10^{15}$ cm^{-2} of TCSE was almost double that of pristine AgNW networks ($n = 5.84 \times 10^{15}$ cm^{-2}); this increase was attributed to the spontaneous redistribution of charges from AgNW (WF = 4.20 eV) to graphene (WF = 4.60 eV). These improvements imply that the graphene layer helps to spread the charge in the electrode.

The charge-injection properties of TCSE were adjusted by using the graphene layer as a WF modifier (Figure 1D). p-Type doping of TCSE using a perfluorosulfonic acid (PFSA, p-dopant) that has a highly electronegative perfluorinated backbone causes a decrease in the electron density in graphene; this shifts the Fermi level E_F toward the valence band.[17] On the contrary, polyethyleneimine (PEI, n-dopant) with a high electron-donating property increases the electron density, and thus creates an interfacial dipole and shifts E_F above the Dirac point.[23] To further increase the electron injection from the n-TCSE to the light-emitting layer, we incorporated an anionic crown CPE that features alternating fluorene and phenylene moieties in a polymeric backbone with alkyl side chains terminated with crown ether or anionic sulfonate groups with tetramethylammonium as a counter ion (Cn6-FPS, simply denoted as Crown-CPE hereafter, synthesis, and characterization described in experimental procedure, Figures S1 and S2, Supporting Information).

The presence of graphene on top of TCSE was first confirmed by cross-section transmission electron microscopy (TEM) (**Figure 2**A). Compared with the backside of the AgNW network as a reference, the high contrast on the surface of AgNW was proven to be graphene. Successful transfer of graphene to the substrate was also confirmed using Raman spectroscopy (Figure S3, Supporting Information). Two characteristic peaks of graphene at 1587 cm^{-1} (G band) and 2684 cm^{-1} (2D band) were observed in the TCSE,[24] confirming that the transfer of graphene to SEBS elastomer matrix was successful and did not induce additional defects.

The pristine TCSE had the same WF = 4.60 eV as the graphene rather than as AgNW (WF = 4.20 eV); this result implies that the graphene layer strongly affects the surface modification of TCSE (Figure 2B). With the deposition of p-type dopant PFSA on top, the interfacial dipole caused by the electronegative perfluorinated backbone substantially reduced the electron density and increased the WF from 4.60 to 5.69 eV; this change can substantially increase the hole-injection capability of TCSE as the anode. PEI was used as the n-dopant to reduce the WF of TCSE as cathode, and neutral amine groups in PEI primarily contribute to the formation of interfacial dipole and reduction of WF.[23] Even though an n-TCSE with low WF = 4.04 eV was achieved, a large electron injection barrier persisted at the interface between n-TCSE and light-emitting polymer

(Super Yellow, PDY-132) that has a lowest unoccupied molecular orbital (LUMO) of 2.8 eV.

The WF of n-TCSE was further reduced by covering its top with anionic Crown-CPE. Modulation of WF with the incorporation of Crown-CPEs containing a π-delocalized main backbone and ionic side chains has been reported previously.[25–28] The negatively charged sulfonate ions and positive tetramethylammonium counter ions in Crown-CPE are self-oriented on top of n-TCSE to create interfacial dipoles which decrease its WF.[25] Evenly dispersed sulfur atoms (with an atomic percentage of ≈0.3%) from sulfonate ions of Crown-CPE in the energy-dispersive spectroscopy (EDS) mapping indicate the uniform distribution of Crown-CPEs on top of n-TCSE (Figure S4A,B, Supporting Information). In addition, the crown ether groups in the side chains have the capability of introducing hydrogen bonding (H-bonding) interactions between the oxygen (in crown ether) and amine groups in PEI. The X-ray photoelectron spectroscopy (XPS) measurements show a binding energy shift of O1s (from 533.3 to 534.1 eV) and N1s signals (from 400.1 to 400.8 eV) with increasing the Crown-CPE thickness from 0 to 6.5 nm, demonstrating the H-bonding interaction between the crown ethers in CPE and amine groups in PEI (Figure S5, Supporting Information). H-bonding interaction was also confirmed using ^{1}H nuclear magnetic resonance (NMR) spectroscopy. Due to the complexity of the Crown-CPE spectra, we first carried out the experiment with 2-hydroxyethyl-18-crown-6 (crown-18) and PEI (Figure S6A, Supporting Information). Protons close to amines (H^a) in PEI show multiple peaks at $\delta = 2.35$–2.65 ppm which get slightly de-shielded and become brooder after mixing Crown-18 in DMSO-d_6 (Figure S6B, Supporting Information). Moreover, the peaks for the protons close to oxygen in Crown-18 (H^b at 3.36–3.70 ppm) also become broader. Similar trends were also observed by mixing PEI into Crown-CPE solution, indicating that the electronegative oxygen atoms in crown ether form H-bonding with the amines in PEI (O···H−N) (Figure S6C, Supporting Information). As a result, the Crown-CPE polymers are expected to show self-oriented ionic moieties due to the H-bonding with PEI, thereby creating a strong interfacial dipole (Figure S7, Supporting Information).

With the net interfacial dipole created at the interface, Kelvin probe mapping revealed that the WF of n-TCSE decreased from 4.04 to 3.63 eV after Crown-CPE coating as a result of vacuum level shift (Figure 2B). The abrupt downward shift of the vacuum level by the additional interfacial dipole created by Crown-CPE was confirmed using ultraviolet photoelectron spectroscopy (UPS) with WF reduced from 3.91 to 3.57 eV which is the lowest WF value among all reported stretchable electrodes (Figure 2C). The significant reduction in WF by ≈1 eV, therefore, substantially increases the electron injection property and the device efficiency. To our best knowledge, this is the first demonstration of a TCSE that has WF in a wide range between 3.57 eV and 5.69 eV (Table S2, Supporting Information).

Besides, maintaining the electrical contact between AgNW and graphene is vital to achieving excellent stretchability. To strengthen the interactions at the AgNW/AgNW and AgNW/graphene interfaces to increase stretchability, junctions of AgNWs were welded using 0.5 mg mL^{-1} graphene
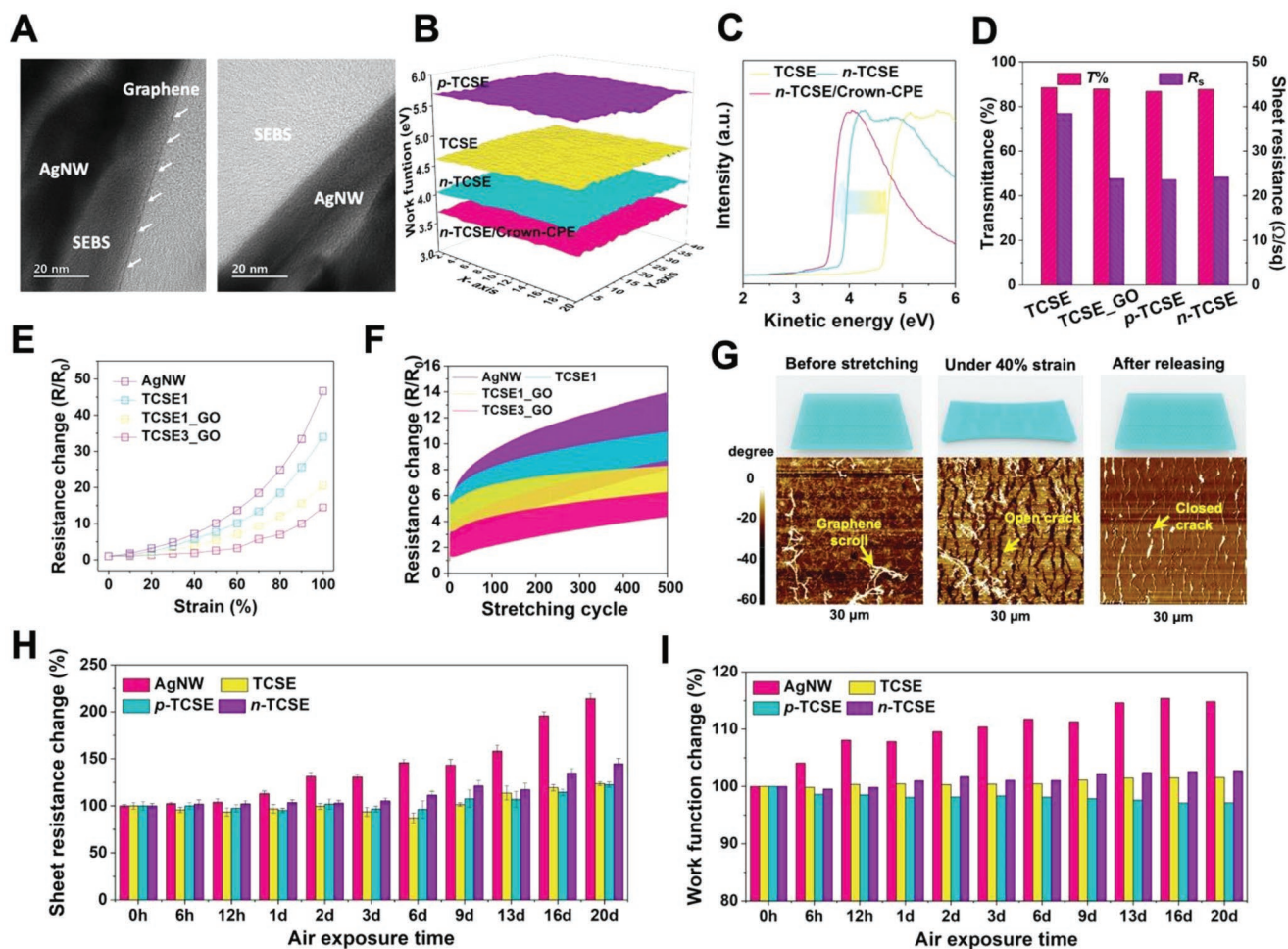
Figure 2. A) Transmission electron microscopy (TEM) cross-section images of TCSE. B) Kelvin probe mapping of WF of TCSE before and after molecular doping using PFSA (p-TCSE), PEI (n-TCSE), and PEI/Crown-CPE (n-TCSE/Crown-CPE). C) The secondary cut-off position of TCSE, n-TCSE, and n-TCSE/Crown-CPE measured using ultraviolet photoelectron spectroscopy (UPS). D) Transmittance T and sheet resistance R_s of pristine TCSE, TCSE with GO treatment, and TCSE after p- and n-type doping. E,F) Static and cyclic stretching tests (strain = 40%) of AgNW, TCSE, and TCSE with multiple layers of graphene before and after graphene oxide (GO) treatment. G) Atomic force microscopy (AFM) phase images taken during the in situ stretching test (strain = 40%) on graphene that had been transferred onto SEBS. H,I) Environmental stability test on AgNW, TCSE, and p- and n-TCSE in terms of R_s and WF change at room temperature and relative humidity of 40%.

oxide (GO) dispersed in co-solvent of IPA and deionized water (DIW) (1:1 v:v) before the embedding process. Despite the insulating nature of GO,[29] the sheet resistance R_s of the AgNW/graphene electrode was reduced from 38 to 24 Ω sq^{-1} after dipping the electrode in GO solution for 0.5 min (Figure S8, Supporting Information). With an increase in GO dipping time, R_s increased to 31 Ω sq^{-1}, whereas the transmittance T remained at ≈89% with little change. The variation in R_s after GO-solution welding can be explained using the atomic force microscopy (AFM) topography of the AgNW/graphene surface (Figure S9A,B, Supporting Information). Given the radius ≈30 nm of AgNWs, the capillary effect drives GO solution to fill the gaps of the AgNWs after 0.5 min of the treatment.[30] With a further increase in treatment time to 1.0 min, continuous and rigid GO thin film that had Young's modulus Y = 32 GPa[31] formed on the AgNW network surface and degraded the mechanical stability of the electrode. Hence, 0.5 min of GO solution welding was chosen as the standard condition for junction welding.

The TCSE with a monolayer of graphene and graphene scrolls after the embedding process had low R_s = 24 Ω sq^{-1} and high T = 89% (Figure 2D), which is almost comparable with that of AgNW/graphene electrodes on glass (Figure S8, Supporting Information). This result indicates a complete transfer of AgNW/graphene onto the SEBS surface without residuals on glass releasing substrate. Neither R_s nor T were significantly changed by p-type or n-type doping of TCSE using PFSA and PEI, respectively.

The mechanical stability of TCSE was then evaluated using a static tensile test (Figure 2E). As expected, the TCSE with one layer of graphene with graphene scrolls (TCSE1) is more mechanically stretchable than pristine AgNW embedded in SEBS. The best stretchability was achieved using a triple layer of graphene with graphene scroll (TCSE3, R_s = 23.2 Ω sq^{-1} and T = 84%); the combination only had a normalized resistance change (R/R_0) of 1.8 at strain = 40%. The same trend was also observed in the cyclic stretching test at strain = 40% for

**ADVANCED
SCIENCE NEWS**

www.advancedsciencenews.com

**ADVANCED
MATERIALS**

www.advmat.de

500 cycles (Figure 2F). The crumpling and interplay among multiple graphene layers can significantly reduce the Young's modulus, and hence increase the stretchability.[32,33]

Graphene is known to readily crack at strain <5% because it has a strong carbon–carbon network that lacks a means of energy dissipation. Counterintuitively, intercalation of graphene scrolls could bridge the cracks to decrease the graphene layer's Young's modulus Y and increase the stretchability.[33] The graphene with graphene scrolls was first transferred onto the glass substrate and then embedded into the elastomer matrix after releasing process. Under strain = 40%, open cracks formed in the graphene layer, but graphene scrolls bridged them to maintain conduction paths (Figure 2G). AgNW percolation networks beneath the graphene can also bridge the cracks to maintain the electrical conductivity under stretching, so TCSE is more stretchable than pristine AgNW networks.

Then, the environmental stability of the pristine AgNW, TCSE, p-TCSE, and n-TCSE were evaluated by monitoring relative changes in R_s and WF at room temperature and relative humidity of 40% (Figure 2H,I). During exposure to these conditions for 20 d, the AgNW electrode was easily oxidized so its R_s increased by >114%, and its WF increased by 15%. Oxidation of AgNW yields Ag_2O,[34] which is nonconductive. However, incorporation of graphene on top of AgNW significantly improved the stability of TCSE. A layer of sp^2-hybridized carbon atoms in a hexagonal lattice can significantly block direct pathways of oxygen and water penetration, and this blockage decreases the oxidation of the AgNWs. After 20 d of exposure to air, p-doping with PFSA exhibited negligible changes in the WF and R_s of the p-TCSE, because PFSA has remarkable chemical stability.[35] Similarly, n-doping with PEI also exhibited better storage stability than that of pristine AgNW electrodes (Figure 2H,I). Hence, the environmental stabilities of p- and n-TCSE are sufficient to meet the processing standard for the electrode for the ISOLEDs.

A surface-modified TCSEs was then prepared for the lamination process. Both stretchable hole-injection layer (SHIL) and light-emitting layer (SEML) were prepared with the addition of 5 and 20 wt% of Triton X-100 into the conducting polymer and the light-emitting polymer, respectively. However, the huge contact angle (CA) difference results in significant differences in wetting properties between the SEML ($CA = 90.0°$) and PEI ($CA = 7.6°$, used as an adhesion promoter onto TCSE), making the laminated interface extremely vulnerable to external stress (Figure S10, Supporting Information). However, no protocols related to ISOLED's fabrication and optimization process have been established before, which makes the highly efficient ISOLED extremely challenging. Therefore, a pressure-controlled method was developed to achieve good electrical contact. To quantify the stress, numbers are labeled on the knob. The number of rotations of the knob was represented by R (Figure S11, Supporting Information).

Lamination quality is also affected by the interchain distance at the laminated interface, which was determined by the pressure that was applied during lamination. A sufficient pressure at an elevated temperature can improve lamination quality. However, high pressure applied to the device may irreversibly degrade the fluorescent properties of the light-emitting layer and the electroluminescence of the device,[36] so measurement

of the photoluminescence (PL) is a powerful tool to find the threshold pressure to balance lamination quality and degradation. PL was measured from the anode side of the ISOLED after lamination; this measurement was possible because the TCSE electrode is highly transparent in the visible range (**Figure 3**A). The cathode n-TCSE was pre-contacted to the p-TCSE coated with the SHIL (Triton X-100 treated PEDOT:PSS) and SEML, then they were hot-pressed together to laminate the interface (Figure S12, Supporting Information).

Lamination time was then fine-tuned at $1.5R$ pressure and 100 °C. With the active layer sandwiched between the TCSEs, PL intensity decreased continuously, as a result of a predominant quenching effect of the TCSE rather than the degradation of the SEML by the lamination (Figure 3B). When only the SEBS substrate was used, the PL intensity of the ISOLED almost doubled; this result implies that the electrode-induced PL quenching effect had been eliminated (Figure 3C). The maximum PL intensity at $1.5R$ was observed after 3 min of lamination. When $2.0R$ was applied, the trend was similar, but the maximum PL intensity was obtained after 1 min of lamination (Figure S13A,B, Supporting Information). Therefore, the lamination time at $1.5R$ and $2.0R$ should be <3 min.

Then the electrode stability under these pressure conditions was evaluated using a current–voltage ($I–V$) scan from −2 to 2 V. PEI was the adhesion promoter sandwiched between two TCSEs to strengthen the adhesion between the substrates (Figure 3D). Pressure of $2.0R$ led to a decrease in the slope of the $I–V$ curve, whereas $1.5R$ caused negligible degradation (Figure 3E,F). The difference was caused by local melting of AgNW networks under elevated temperature and pressure; this response is a result of the high surface-to-volume ratio of NWs.[37] Therefore, the finalized lamination temperature, and pressure conditions of ISOLEDs were 100 °C, and $1.5R$ (≈50 kPa) for 3 min, respectively. The in situ stretching test on the ISOLED identified a crack onset strain of ≈73% (Figure S14, Supporting Information), which is sufficient for the ISOLED.

Before the ISOLED fabrication, the AgNW/graphene on the glass was patterned using a photoresist-free reactive ion etching (RIE) method, then embedded in the SEBS elastomer matrix. The graphene layer can also serve as a sacrificial layer that is easily etched by the oxygen plasma and washed away after the patterning process (Figure S15, Supporting Information). The electrode then was embedded in SEBS and used as the electrode for ISOLEDs.

The flat-band energy diagram of the ISOLED was displayed with respect to the vacuum level (**Figure 4**A). Efficient electron injection is always challenging without using reactive metals or metal fluorides (e.g., Ca, Ba, Cs, LiF, BaF_2 or CsF) as the interlayer underneath an Al or Ag layer, because of a large electron injection barrier between pristine TCSE and the LUMO = 3.20 eV of the SEML. Formation of the strong net interfacial dipole after consecutive deposition of PEI and Crown-CPE can substantially downshift the vacuum level and reduce the WF from 4.60 to 3.57 eV; this change could significantly increase the electron injection capability and improve the balance of charge injection.

The light-emitting characteristics were first evaluated on a rigid ITO electrode without using any reactive alkali metals as the electron injection layer (Figure 4B). Use of the Crown-CPE
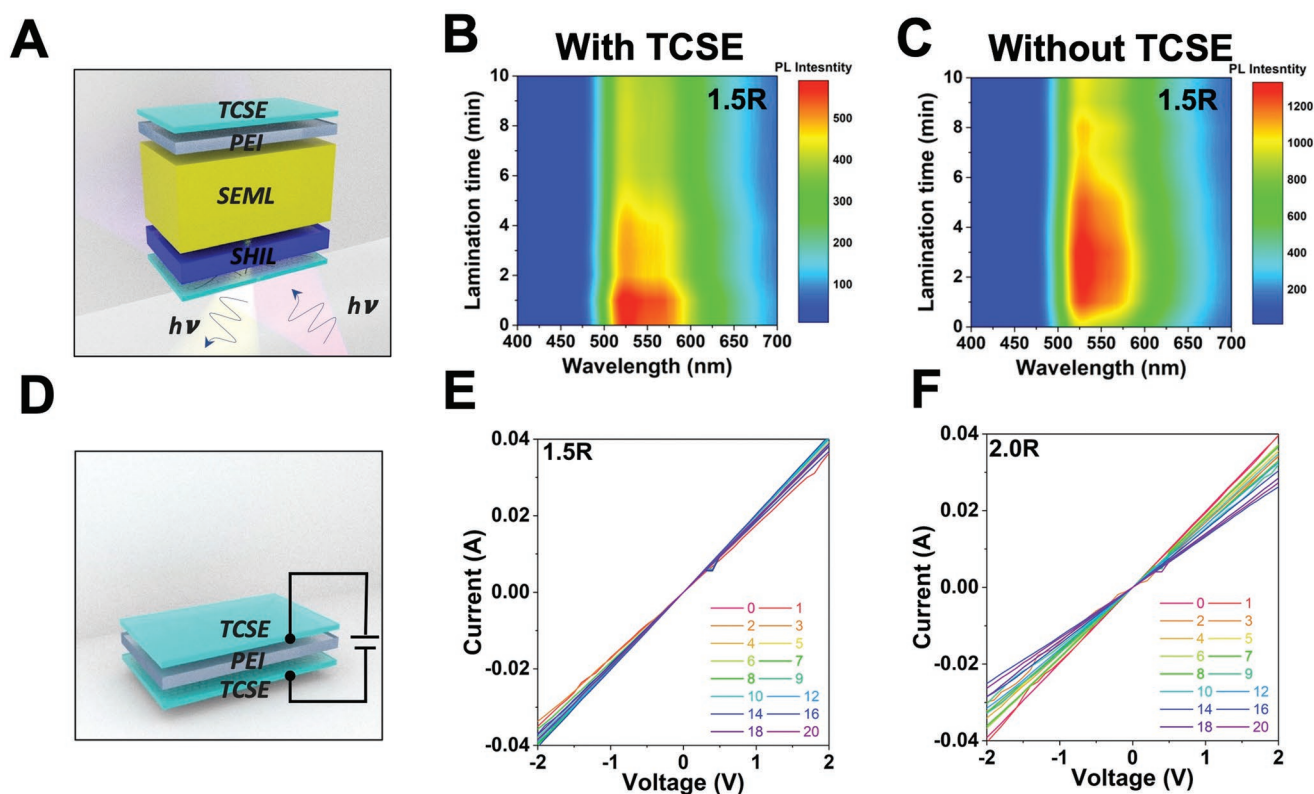
**ADVANCED
SCIENCE NEWS**

www.advancedsciencenews.com

**ADVANCED
MATERIALS**

www.advmat.de

Figure 3. A) Schematic illustration of the device structure for evaluation of lamination quality using photoluminescence (PL). B,C) Photoluminescence (PL) color plots with and without using TCSE after applying increasing time of lamination at 1.5R pressure. D) Schematic illustration of the device structure for evaluation of electrode stability using current–voltage (*I–V*) curve. E,F) *I–V* curve with increasing lamination time from 0 to 20 min at 1.5R and 2.0R.

as the dipole layer could simultaneously increase both current density and luminance, so the device show maximum luminance L_{max} = 9914 cd/m^2 and a low turn-on voltage V_{on} = 3.4 V. Due to the conjugated backbone of Crown-CPE and induced interfacial dipole at the electrode interface, the electron injection capability was significantly improved as expected. The ISOLED with the Crown-CPE interfacial dipole layer had similar responses: L_{max} = 2185 cd m^{-2} and V_{on} = 5.3 V; these results imply that 2D electrical contact is formed at the n-TCSE interface after the lamination process.

In Super Yellow, holes are more mobile than electrons,[38] so the rate of charge injection is dominated by hole transport. As a result, charge imbalance arises due to limited electron injection, so the maximum CE of ITO devices was achieved at L = 4223 cd m^{-2} with CE = 6.47 cd A^{-1} (Figure 4C). The low endurance of AgNWs in the TCSE against local joule heating makes the ISOLED vulnerable upon applying high electric field. The resultant ISOLED showed the maximum CE = 20.3 cd A^{-1} at only 119.2 cd m^{-2} (Figure 4C). To prove the spontaneous formation of interfacial dipole due to the Crown-CPE, time-dependent capacitance and current of ITO devices were analyzed at varying voltages from 2 to 5 V. Neither capacitance nor current showed any significant time-dependent variations in the ITO devices; this result implies that the Crown-CPE-induced dipole layer formed spontaneously without the effect of drift voltage (Figure 4D). The device using Crown-CPE showed an increase in capacitance at V < 2 V; this change was attributed

to the accumulation of both electrons and holes at the SEML interfaces, and also proves that charge injection is efficient at low voltages (Figure 4E).

Then the lifetime of ISOLED was tested in a constant-current mode until failure in a glove box, starting with a luminance of 100 cd m^{-2}. The lifetime to 50% of initial luminance under continuous operation was 7.07 h (Figure S16, Supporting Information). Both efficiency and lifetime were substantially improved compared to a reported ISOLED that uses the same intrinsically stretchable emitting layer.[15] Therefore, designing appropriate stretchable electrode materials with an optimized device architecture is vital to achieving bright and stable ISOLEDs with high efficiency. The stretching tolerance of the ISOLED unit cell was measured by sandwiching it between 3M VHB tapes as encapsulation. The initial luminance of the ISOLED unit cell decreased to 71.8% after the application of strain = 20% and kept decreasing with further stretching (Figure 4F).

To the best of our knowledge, this is the highest efficiency achieved in the ISOLEDs that have been fabricated without using any vacuum process (Figure 4G). To demonstrate the feasibility of TCSE and the optimized lamination process for large-scale application, a 3 inch five-by-five matrix passive-matrix ISOLED was demonstrated. It was loaded on a home-made convex stretching machine and fixed using a frame with magnets on the corners (Figure S17, Supporting Information). The linear strain induced on the surface of the substrate was calculated from the increase in the length of the arc created
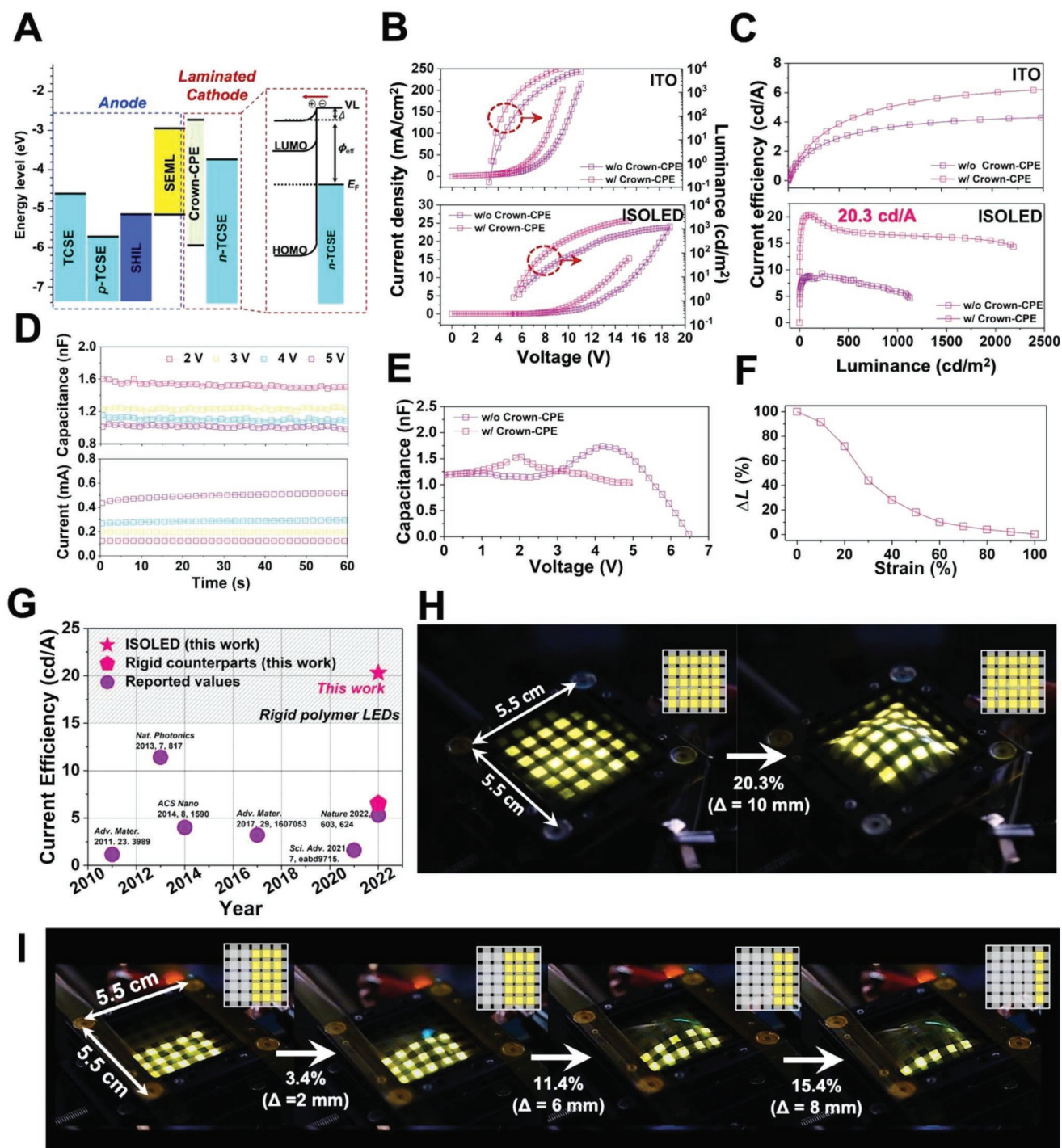
Figure 4. A) Flat-band energy level diagram of the ISOLED with respect to the vacuum level. The rectangle in red highlights the n-TCSE/Crown-CPE interface with the downward band bending induced by the strong interfacial dipole of Crown-CPE and PEI. B) Current density–voltage–luminance (J–V–L). C) Current efficiency–luminance characteristics of ISOLED and their rigid counterparts based on ITO with or without using the Crown-CPE interlayer. D) Time-dependent measurement of capacitance and current on ITO-based rigid devices in B) under increasing voltages from 2 to 5 V. E) Capacitance–voltage characteristic ITO-based rigid devices with or without using as the Crown-CPE interlayer. F) Change in luminance of ISOLED at 6 V versus strain. G) Progress in the development of intrinsically stretchable LED. Current efficiency of 15 cd A^{-1} represents the typical efficiency of rigid polymer LED fabricated using an ITO anode and a metal cathode. H,I) Convex stretching of three-inch five-by-five passive matrix ISOLED by using a hemispherical stylus with a radius of 20.5 mm (moving upward for 10 mm ≈20% linear strain).

by the hemisphere with a radius of 20.5 mm when compared with the corresponding chord in the hemisphere (Table S3, Supporting Information). The passive matrix ISOLED showed

a stable light-emission even at strain = 20%, applied by convex stretching (Figure 4H, Movie S1, Supporting Information). The matrix can also be operated under convex stretching

under different applying voltages (Figure 4I). This is the first demonstration on a large scale of passive-matrix ISOLEDs that tolerate significant convex stretching.

3. Conclusion

A highly efficient ISOLED was designed using graphene-based TCSEs as both electrodes to overcome the intrinsic charge injection limitation at the interface between 1D AgNW/organic layer. A graphene layer with graphene scrolls has high carrier mobility $m = 519.27 \pm 0.32$ cm^2 V^{-1} s^{-1}) was introduced to form a complete 2D interface. The electron injection from TCSE can be significantly increased after introducing a strong dipole moment by incorporating an anionic Crown-CPE that has self-aligned ionic moieties on the n-TCSE. Efficient hole injection was established with p-type molecular doping using PFSA. To our best knowledge, this is the first demonstration of a stretchable electrode that has a tunable WF in a wide range between 3.57 and 5.69 eV. As a consequence of efficient electron and hole injection from both TCSEs after pressure-controlled lamination, the ISOLEDs achieved an unprecedently high CE = 20.3 cd A^{-1}, which is the highest reported efficiency among all ISOLEDs. Using these tactics, a three-inch five-by-five matrix passive matrix ISOLED also proves the feasibility of the TCSE for large-scale applications. This work has provided a design protocol for highly efficient stretchable optoelectronic devices with engineered intrinsically stretchable materials and favorable interfacial electronic structures. In the future, use of phosphorescent or thermally activated delayed fluorescent (TADF) materials with stretchable polymer hosts may achieve CE that even exceeds the high value reported here.

Supporting Information

Supporting Information is available from the Wiley Online Library or from the author.

Conflict of Interest

The authors declare no conflict of interest.

Data Availability Statement

The data that support the findings of this study are available from the corresponding author upon reasonable request.

[1] Y. Lee, J. W. Chung, G. H. Lee, H. Kang, J.-Y. Kim, C. Bae, H. Yoo, S. Jeong, H. Cho, S.-G. Kang, J. Y. Jung, D.-W. Lee, S. Gam, S. G. Hahm, Y. Kuzumoto, S. J. Kim, Z. Bao, Y. Hong, Y. Yun, S. Kim, *Sci. Adv.* **2021**, *7*, eabg9180.

[2] S. Lee, D. Sasaki, D. Kim, M. Mori, T. Yokota, H. Lee, S. Park, K. Fukuda, M. Sekino, K. Matsuura, T. Shimizu, T. Someya, *Nat. Nanotechnol.* **2019**, *14*, 156.

[3] I. You, D. G. Mackanic, N. Matsuhisa, J. Kang, J. Kwon, L. Beker, J. Mun, W. Suh, T. Y. Kim, J. B.-H. Tok, Z. Bao, U. Jeong, *Science* **2020**, *370*, 961.

[4] N. Matsuhisa, S. Niu, S. J. K. O'Neill, J. Kang, Y. Ochiai, T. Katsumata, H.-C. Wu, M. Ashizawa, G.-J. N. Wang, D. Zhong, X. Wang, X. Gong, R. Ning, H. Gong, I. You, Y. Zheng, Z. Zhang, J. B. H. Tok, X. Chen, Z. Bao, *Nature* **2021**, *600*, 246.

[5] J. Xu, S. Wang, G.-J. N. Wang, C. Zhu, S. Luo, L. Jin, X. Gu, S. Chen, V. R. Feig, J. W. F. To, S. Rondeau-Gagné, J. Park, B. C. Schroeder, C. Lu, J. Y. Oh, Y. Wang, Y.-H. Kim, H. Yan, R. Sinclair, D. Zhou, G. Xue, B. Murmann, C. Linder, W. Cai, J. B.-H. Tok, J. W. Chung, Z. Bao, *Science* **2017**, *355*, 59.

[6] M. S. White, M. Kaltenbrunner, E. D. Głowacki, K. Gutnichenko, G. Kettlgruber, I. Graz, S. Aazou, C. Ulbricht, D. A. M. Egbe, M. C. Miron, Z. Major, M. C. Scharber, T. Sekitani, T. Someya, S. Bauer, N. S. Sariciftci, *Nat. Photonics* **2013**, *7*, 811.

[7] S. Park, S. W. Heo, W. Lee, D. Inoue, Z. Jiang, K. Yu, H. Jinno, D. Hashizume, M. Sekino, T. Yokota, K. Fukuda, K. Tajima, T. Someya, *Nature* **2018**, *561*, 516.

[8] L. Zhou, M. Yu, X. Chen, S. Nie, W.-Y. Lai, W. Su, Z. Cui, W. Huang, *Adv. Funct. Mater.* **2018**, *28*, 1705955.

[9] D. Li, X. Liu, X. Chen, W.-Y. Lai, W. Huang, *Adv. Mater. Technol.* **2019**, *4*, 1900196.

[10] Z. Zhang, K. Guo, Y. Li, X. Li, G. Guan, H. Li, Y. Luo, F. Zhao, Q. Zhang, B. Wei, Q. Pei, H. Peng, *Nat. Photonics* **2015**, *9*, 233.

[11] Y. Zhibin, N. Xiaofan, L. Zhitian, P. Qibing, *Adv. Mater.* **2011**, *23*, 3989.

[12] J. Liu, J. Wang, Z. Zhang, F. Molina-Lopez, G.-J. N. Wang, B. C. Schroeder, X. Yan, Y. Zeng, O. Zhao, H. Tran, T. Lei, Y. Lu, Y.-X. Wang, J. B. H. Tok, R. Dauskardt, J. W. Chung, Y. Yun, Z. Bao, *Nat. Commun.* **2020**, *11*, 3362.

[13] J. Liang, L. Li, K. Tong, Z. Ren, W. Hu, X. Niu, Y. Chen, Q. Pei, *ACS Nano* **2014**, *8*, 1590.

[14] J. Liang, L. Li, X. Niu, Z. Yu, Q. Pei, *Nat. Photonics* **2013**, *7*, 817.

[15] J. H. Kim, J. W. Park, *Sci. Adv.* **2021**, *7*, eabd9715.

[16] Z. Zhang, W. Wang, Y. Jiang, Y.-X. Wang, Y. Wu, J.-C. Lai, S. Niu, C. Xu, C.-C. Shih, C. Wang, H. Yan, L. Galuska, N. Prine, H.-C. Wu, D. Zhong, G. Chen, N. Matsuhisa, Y. Zheng, Z. Yu, Y. Wang, R. Dauskardt, X. Gu, J. B. H. Tok, Z. Bao, *Nature* **2022**, *603*, 624.

[17] T.-H. Han, Y. Lee, M.-R. Choi, S.-H. Woo, S.-H. Bae, B. H. Hong, J.-H. Ahn, T.-W. Lee, *Nat. Photonics* **2012**, *6*, 105.

[18] P. K. H. Ho, J.-S. Kim, J. H. Burroughes, H. Becker, S. F. Y. Li, T. M. Brown, F. Cacialli, R. H. Friend, *Nature* **2000**, *404*, 481.

[19] T. Cheng, Y. Zhang, W. Y. Lai, W. Huang, *Adv. Mater.* **2015**, *27*, 3349.

[20] D. Li, W. Y. Lai, Y. Z. Zhang, W. Huang, *Adv. Mater.* **2018**, *30*, 1704738.

[21] S. Höfle, A. Schienle, M. Bruns, U. Lemmer, A. Colsmann, *Adv. Mater.* **2014**, *26*, 2750.

**ADVANCED
SCIENCE NEWS**

www.advancedsciencenews.com

**ADVANCED
MATERIALS**

www.advmat.de

[22] H. Zhou, J. Park, Y. Lee, J.-M. Park, J.-H. Kim, J. S. Kim, H.-D. Lee, S. H. Jo, X. Cai, L. Li, X. Sheng, H. J. Yun, J.-W. Park, J.-Y. Sun, T.-W. Lee, *Adv. Mater.* **2020**, *32*, 2001989.

[23] Y. Zhou, C. Fuentes-Hernandez, J. Shim, J. Meyer, A. J. Giordano, H. Li, P. Winget, T. Papadopoulos, H. Cheun, J. Kim, M. Fenoll, A. Dindar, W. Haske, E. Najafabadi, T. M. Khan, H. Sojoudi, S. Barlow, S. Graham, J. L. Bredas, S. R. Marder, A. Kahn, B. Kippelen, *Science* **2012**, *336*, 327.

[24] A. C. Ferrari, D. M. Basko, *Nat. Nanotechnol.* **2013**, *8*, 235.

[25] U. Giovanella, M. Pasini, M. Lorenzon, F. Galeotti, C. Lucchi, F. Meinardi, S. Luzzati, B. Dubertret, S. Brovelli, *Nano Lett.* **2018**, *18*, 3441.

[26] K.-G. Lim, S. M. Park, H. Y. Woo, T.-W. Lee, *ChemSusChem* **2015**, *8*, 3062.

[27] B. H. Lee, I. H. Jung, H. Y. Woo, H.-K. Shim, G. Kim, K. Lee, *Adv. Funct. Mater.* **2014**, *24*, 1100.

[28] C. H. Jang, A. K. Harit, S. Lee, S. H. Kim, J.-E. Jeong, J. H. Park, E. D. Jung, J. M. Ha, S. K. Kwak, H. Y. Woo, M. H. Song, *ACS Nano* **2020**, *14*, 13246.

[29] K. P. Loh, Q. Bao, G. Eda, M. Chhowalla, *Nat. Chem.* **2010**, *2*, 1015.

[30] Y. Liu, J. Zhang, H. Gao, Y. Wang, Q. Liu, S. Huang, C. F. Guo, Z. Ren, *Nano Lett.* **2017**, *17*, 1090.

[31] D. A. Dikin, S. Stankovich, E. J. Zimney, R. D. Piner, G. H. B. Dommett, G. Evmenenko, S. T. Nguyen, R. S. Ruoff, *Nature* **2007**, *448*, 457.

[32] R. J. T. Nicholl, H. J. Conley, N. V. Lavrik, I. Vlassiouk, Y. S. Puzyrev, V. P. Sreenivas, S. T. Pantelides, K. I. Bolotin, *Nat. Commun.* **2015**, *6*, 8789.

[33] N. Liu, A. Chortos, T. Lei, L. Jin, T. R. Kim, W.-G. Bae, C. Zhu, S. Wang, R. Pfattner, X. Chen, R. Sinclair, Z. Bao, *Sci. Adv.* **2017**, *3*, e1700159.

[34] Y. Ahn, Y. Jeong, Y. Lee, *ACS Appl. Mater. Interfaces* **2012**, *4*, 6410.

[35] A. Kusoglu, A. Z. Weber, *Chem. Rev.* **2017**, *117*, 987.

[36] H. Zhou, J.-W. Park, *Org. Electron.* **2015**, *24*, 272.

[37] A. Kim, Y. Won, K. Woo, C.-H. Kim, J. Moon, *ACS Nano* **2013**, *7*, 1081.

[38] T. Lei, J.-H. Dou, X.-Y. Cao, J.-Y. Wang, J. Pei, *J. Am. Chem. Soc.* **2013**, *135*, 12168.